

## APPLIED SCIENCES AND ENGINEERING

## Room temperature multiplexed gas sensing using chemical-sensitive 3.5-nm-thin silicon transistors

Hossain Mohammad Fahad,<sup>1,2,3\*</sup> Hiroshi Shiraki,<sup>1,2,4\*</sup> Matin Amani,<sup>1,2,3</sup> Chuchu Zhang,<sup>1</sup> Vivek Srinivas Hebbar,<sup>1</sup> Wei Gao,<sup>1,2,3</sup> Hiroki Ota,<sup>1,2,3</sup> Mark Hettick,<sup>1,2,3</sup> Daisuke Kiriya,<sup>1,2,3</sup> Yu-Ze Chen,<sup>5</sup> Yu-Lun Chueh,<sup>5</sup> Ali Javey<sup>1,2,3†</sup>

2017 © The Authors, some rights reserved; exclusive licensee American Association for the Advancement of Science. Distributed under a Creative Commons Attribution NonCommercial License 4.0 (CC BY-NC).

There is great interest in developing a low-power gas sensing technology that can sensitively and selectively quantify the chemical composition of a target atmosphere. Nanomaterials have emerged as extremely promising candidates for this technology due to their inherent low-dimensional nature and high surface-to-volume ratio. Among these, nanoscale silicon is of great interest because pristine silicon is largely inert on its own in the context of gas sensing, unless functionalized with an appropriate gas-sensitive material. We report a chemical-sensitive field-effect transistor (CS-FET) platform based on 3.5-nm-thin silicon channel transistors. Using industry-compatible processing techniques, the conventional electrically active gate stack is replaced by an ultrathin chemical-sensitive layer that is electrically nonconducting and coupled to the 3.5-nm-thin silicon channel. We demonstrate a low-power, sensitive, and selective multiplexed gas sensing technology using this platform by detecting H<sub>2</sub>S, H<sub>2</sub>, and NO<sub>2</sub> at room temperature for environment, health, and safety in the oil and gas industry, offering significant advantages over existing technology. Moreover, the system described here can be readily integrated with mobile electronics for distributed sensor networks in environmental pollution mapping and personal air-quality monitors.

## INTRODUCTION

To date, the gas sensor market has primarily been dominated by applications in oil and gas, automotive, and other process industries. This may no longer hold true, especially with the recent boom in low-power sensor technologies associated with the Internet of things. New applications in personal air-quality monitoring, pollution tracking, and breath analysis for preventive health care have created a growing demand for low-power chip-scale gas sensors. Although there are several categories of gas sensors, only three have indicated potential for chip-scale miniaturization and low-power operation, namely, resistive ceramic (1) and metallic (2) sensors, nanoelectromechanical systems (3), and field-effect transistors (FETs) (4). Of these, resistive ceramic gas sensors have been explored extensively in the past. These gas sensors are typically based on transition metal oxides that operate on the principle of resistance change due to gas-oxide redox reactions at high temperatures. Furthermore, resistance change is affected in the same material undergoing chemical change. Selective gas sensing using this technology is quite challenging because it is dependent on the temperature of gas-oxide interaction. By far, the FET technology has shown significant potential in overcoming limitations of size, power consumption, and sensitivity. The FET technology works on the principle of channel current modulation due to gas interaction in the linear amplifying region of a transistor. Strong and growing interest in this technology is very clear, especially with the advent of materials such as carbon nanotubes (5–9), semiconducting nanowires (4, 10–15), organic semiconductors (16–18), graphene (19), and transition metal dichalcogenides (20, 21). Silicon nanowires are of particular relevance

to this work, where significant progress has been made in demonstrating them for gas sensing (4) and biosensing (11), indicating nanoscale silicon as a model material system for sensitive and selective sensors.

Here, we demonstrate chemical-sensitive FETs (CS-FETs) as a highly sensitive, selective, and low-power gas sensing platform, where a 3.5-nm-thin silicon channel on an insulator is the enabling technology (Fig. 1). Today, these ultrathin silicon channels (22) are used as fully depleted transistors to drive the current generation of low-power digital electronics (23). The CS-FET sensors operate at room temperature and are chemically gated with a chemical-sensitive layer, which upon exposure to a target gas, induces a channel threshold voltage shift. Room temperature gas sensors may typically suffer from effects such as poisoning and slow recovery to baseline after gas exposure. To address this, CS-FET gas sensors are integrated with local Au/Cr microheaters on a silicon-on-insulator (SOI) platform. These microheaters are activated only after a gas detection event to assist in quick recovery to baseline and do not contribute in any way to the actual sensing mechanism of the CS-FET. Figure 1A depicts a perspective-view optical microscope image of a fabricated CS-FET sensor, whereas Fig. 1 (B and C) depicts the array concept of individually functionalized CS-FETs and a pictorial representation of a single device, respectively.

## RESULTS

Although the CS-FET is a generic gas sensing technology that can be configured for different applications by selection of proper sensing films, the targeted application for this work is in the detection of H<sub>2</sub>S, H<sub>2</sub>, and NO<sub>2</sub> for personnel and environment safety in the oil and gas industry. H<sub>2</sub>S is a colorless, flammable, and corrosive gas that poses significant safety concerns in this industry. It has a distinct rotten egg smell at very low concentrations [approximately 0.01 to 1.5 parts per million (ppm)] and becomes odorless and toxic beyond this concentration range with instant death at 800 ppm. In the United States, the National Institute for Occupational Safety and Health (NIOSH) has

<sup>1</sup>Department of Electrical Engineering and Computer Sciences, University of California, Berkeley, Berkeley, CA 94720, USA. <sup>2</sup>Berkeley Sensor and Actuator Center, University of California, Berkeley, Berkeley, CA 94720, USA. <sup>3</sup>Materials Sciences Division, Lawrence Berkeley National Laboratory, Berkeley, CA 94720, USA. <sup>4</sup>Murata Manufacturing Co. Ltd., Nagaokakyo, Kyoto 617-8555, Japan. <sup>5</sup>Department of Materials Science and Engineering, National Tsing Hua University, Hsinchu, Taiwan 30013, R.O.C.

\*These authors contributed equally to this work.

†Corresponding author. Email: ajavey@eecs.berkeley.edu

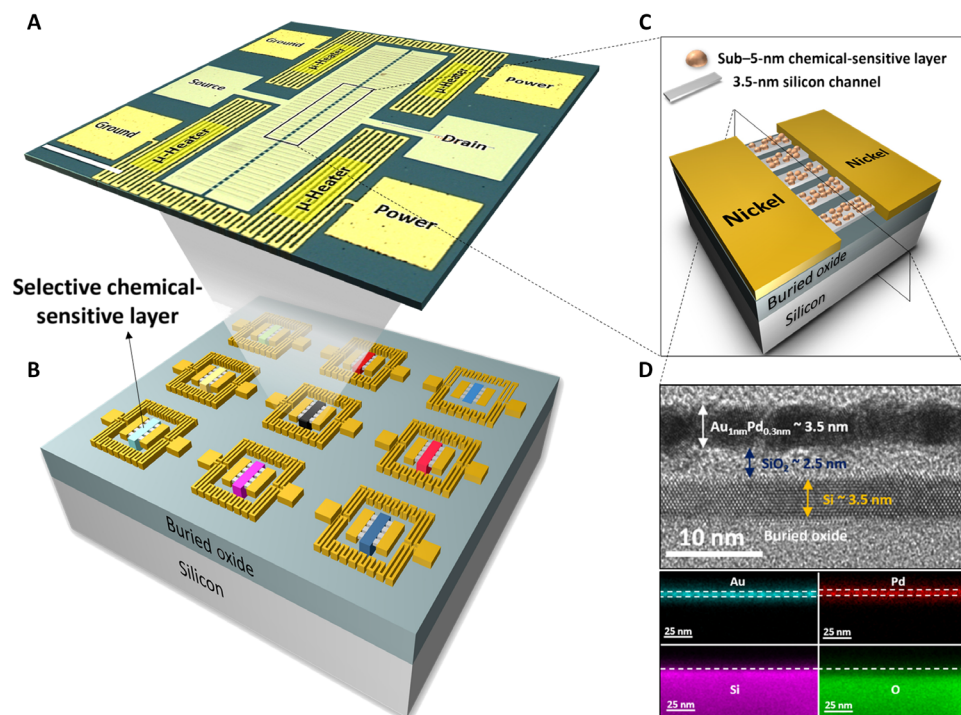


**Fig. 1. Schematic illustrations and detailed images of a CS-FET chip.** (A) Optical microscope image of a single CS-FET functionalized with a Pd-Au sensing layer integrated with microheaters. (B) Schematic illustration of a single-chip CS-FET array functionalized with different selective sensing layers. (C) Detailed zoomed-in representation of a single CS-FET. (D) Cross-sectional TEM image taken across the ultrathin silicon channel as shown in (C) with the associated EDS indicating the elemental composition of a single Pd-Au CS-FET. Scale bars, 250  $\mu\text{m}$ .

characterized a 60-min exposure to 100 ppm of  $\text{H}_2\text{S}$  as an immediately dangerous to life or health (IDLH) condition (24). Because of this, the  $\text{H}_2\text{S}$  sensing range of interest in the oil and gas industry is 0 to 100 ppm. The state of the art uses a combination of resistive ceramic and electrochemical  $\text{H}_2\text{S}$  sensors, with response times ( $t_{90}$ ) of around 15 to 120 s and detection limits of 0.4 to 20 ppm, depending on the manufacturer. Similar to  $\text{H}_2\text{S}$ ,  $\text{H}_2$  is also a major concern in these industries, where it is used in petroleum refining that involves desulfurization. NIOSH characterizes  $\text{H}_2$  as a flammable gas with a lower explosion limit of 4% by volume in air (24). Catalytic-type as well as optical infrared sensors are currently used for detecting  $\text{H}_2$  leaks with response times of around 30 s or less and detection ranges of 0 to 100%. In addition to  $\text{H}_2\text{S}$  and  $\text{H}_2$ ,  $\text{NO}_2$  emissions from such industries are becoming increasingly important to monitor because they are common indicators of air quality.  $\text{NO}_2$ , which is a respiratory irritant, is a reddish brown gas with a pungent odor that is released during the burning of complex hydrocarbons. The IDLH limit for  $\text{NO}_2$ , as specified by NIOSH, is 20 ppm for a 30-min exposure (24). The sensing range of interest is also 0 to 100 ppm, and the state of the art uses both resistive ceramic and electrochemical gas sensor technology. Depending on the specific manufacturer, response times are around a minute or less with detection ranges of 0.2 to 20 ppm.

The technologies described above are typically very bulky in size and weight as well as power-hungry, rendering them mostly as fixed point detectors. It is also quite common for these sensors to detect false positives due to cross-sensitivity from interfering gases. The effective sensing of  $\text{H}_2\text{S}$  is of importance to personnel health and safety in the oil and gas industry, where the current standard practice is for personnel to carry bulky and power-hungry monitors to detect the presence

of the mentioned gases. In the following sections, we demonstrate that the CS-FET gas sensor technology can offer significant advantages in terms of sensitivity, selectivity, size, and power consumption that can augment or potentially replace existing technology.

CS-FETs are gated chemically with gas-specific ultrathin sensing layers (sub-5 nm) that are electrically nonconductive. Interactions with a target gas induce changes in the sensing layer work function, which in turn causes large modulations in the current ( $I_D$ ) flowing through the ultrathin silicon channel, leading to highly sensitive detection events. Unlike other highly sensitive nanomaterials, the CS-FET silicon channel on its own is comparatively inert and unresponsive unless functionalized with appropriate sensing layers, enabling selective detection (see fig. S1). Depending on the nature of the target gas, sensing layers can be composed of metal or metal alloys, transition metal oxides, or even polymers. Here, mono- and bimetallic composites are used as chemical-sensitive layers. The underlying transistors in the CS-FET platform are fabricated using a complete top-down approach, which is fully compatible with silicon complementary metal-oxide semiconductor (CMOS) processing (23). This enables scalable batch fabrication of large ultrathin channel transistor arrays, where each transistor can be functionalized with different gas-specific sensing layers (Fig. 1B), paving the way to single-chip multiplexing for selective gas sensing. Selectivity is a major challenge in any gas sensing technology. It is the property by which a gas sensor can accurately detect the presence of a specific gas in the presence of other interferents. Although absolute selectivity may be difficult to achieve, relative selectivity is highly possible if selectivity is defined contextually, that is, previous knowledge of known interferents in a targeted application or environment (25).

Using multiplexed CS-FETs, we show that it is possible to actively track and detect the gases of the target application described earlier, sensitively and selectively at low power. By iterative elimination, three sensing layers were identified for the abovementioned three gases of interest and deposited on individual CS-FETs: Pd<sub>0.3nm</sub>Au<sub>1nm</sub> for H<sub>2</sub>S, Ni<sub>0.3nm</sub>Pd<sub>1nm</sub> for H<sub>2</sub>, and Ni<sub>1nm</sub> for NO<sub>2</sub>. As described in the previous section, all three CS-FET gas sensors in this work operate at room temperature. Figure 1D shows a cross-sectional transmission electron microscopy (TEM) image and an associated energy-dispersive x-ray spectroscopy (EDS) profile of a completed device with an ultrathin composite sensing layer of Pd-Au capacitively coupled to a 3.5-nm-thin silicon channel (see also fig. S2). This CS-FET (discussed below) is sensitive to the detection of H<sub>2</sub>S.

In terms of device operation, the CS-FET works as a junctionless n-channel transistor, with the channel degenerately n-doped to similar levels as the source and the drain (26). Most charge carriers in the 3.5-nm-thin silicon channel can be fully depleted upon gas exposure, leading to large modulations in the output current. Sensing principle in the CS-FET is based on the channel threshold voltage shift ( $V_t$  shift), depicted in Fig. 2 (A and B) by a simplified band alignment representation across the sensing layer and silicon channel before and after exposure to a target gas (in this case, H<sub>2</sub>S). Gas interaction with the Pd-Au sensing layer can lead to a change in its work function ( $\phi_m$ )

as well as charge density. This net change increases the channel potential, leading to a decrease in device threshold voltage (more negative  $V_t$ ) and an increase in  $I_D$ . Sensing is highly dependent on the nature of the interacting gas and the sensing layer, decreased  $V_t$  for reducing gases (for example, H<sub>2</sub>S) and increased  $V_t$  for oxidizing gases (for example, NO<sub>2</sub>). Diagnostic back gate measurements ( $I_D$  versus  $V_{BG}$  and  $I_D$  versus  $V_{DS}$ ) in Fig. 2 (C and D) experimentally validate this  $V_t$  shift sensing principle upon targeted gas exposure.

Figure 3A shows time-dependent measurements of the Pd-Au-based H<sub>2</sub>S sensor operated at a supply voltage of 100 mV. With a sampling time of 1 s, the baseline current is ~30 nA, leading to a low standby power consumption of ~3 nW. This particular sensor has a very low detection limit of 1 part per billion (ppb) with a saturation concentration of above 10 ppm. The response versus concentration curve (Fig. 3B) shows a linear region from 1 to 10 ppm with a sensitivity of 280%/ppm [ $(\Delta G/G_0)$  per ppm]. This high sensitivity is attributed to the thin sensing layer as well as the thin silicon channel (as illustrated in fig. S3, thick silicon channel junctionless transistors results in a much lower sensitivity). Response times ( $t_{90}$ ; time taken by the sensor current to reach 90% of its maximum value upon exposure to gas) are longer for smaller gas concentrations, with ~144 s for 1 ppb of H<sub>2</sub>S and ~112 s for 100 ppm of H<sub>2</sub>S. Microheater-assisted recovery times ( $t_{50}$ ; time taken by the sensor current to drop to within 50% of its

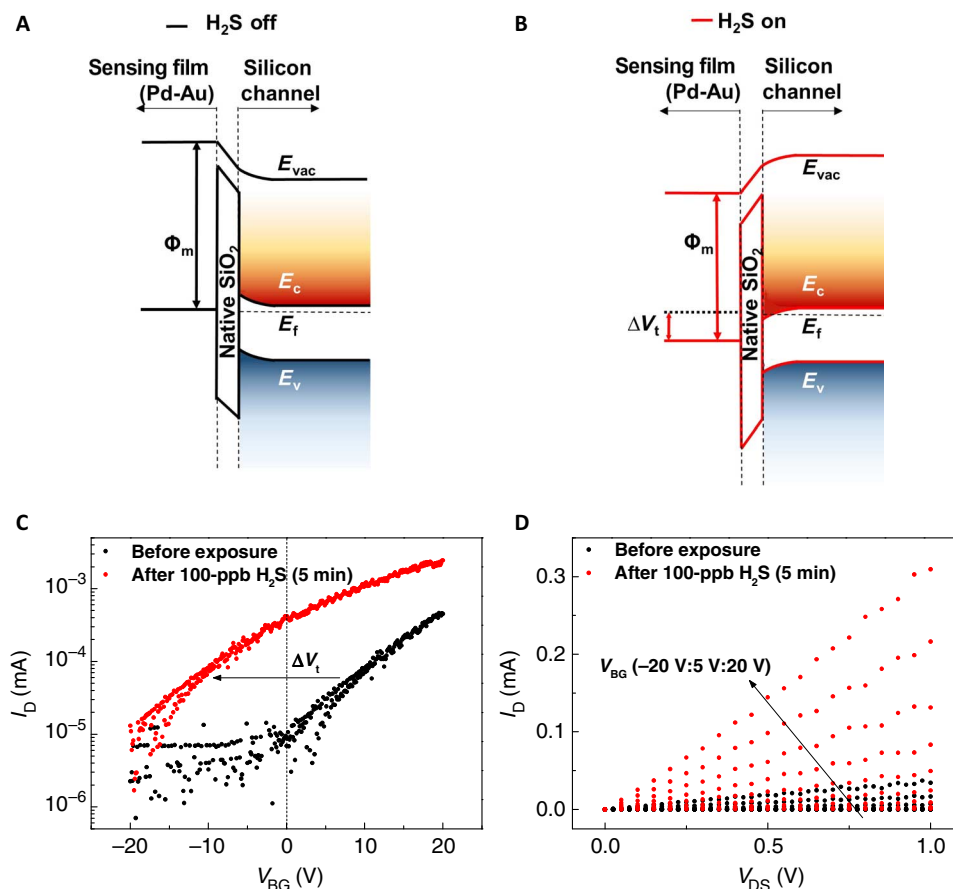


**Fig. 2. Sensing mechanism of CS-FETs.** Schematic illustration of the band edge alignment across Pd-Au sensing layer and ultrathin silicon channel in a H<sub>2</sub>S-sensitive CS-FET (A) before H<sub>2</sub>S exposure and (B) after 100 ppb of H<sub>2</sub>S exposure.  $E_{vac}$ , vacuum energy level;  $E_c$ , bottom of the silicon conduction band energy level;  $E_v$ , top of the silicon valence band energy level;  $E_f$ , silicon Fermi-level energy. (C) Experimental transfer characteristics ( $I_D$ - $V_{BG}$ ) of a H<sub>2</sub>S-sensitive CS-FET demonstrating  $V_t$  shift before and after 100-ppb H<sub>2</sub>S (in air) exposure ( $V_{DS} = 10$  mV). (D) Experimental output characteristics ( $I_D$ - $V_{DS}$ ) before and after 100 ppb of H<sub>2</sub>S (in air) exposure of the same CS-FET.

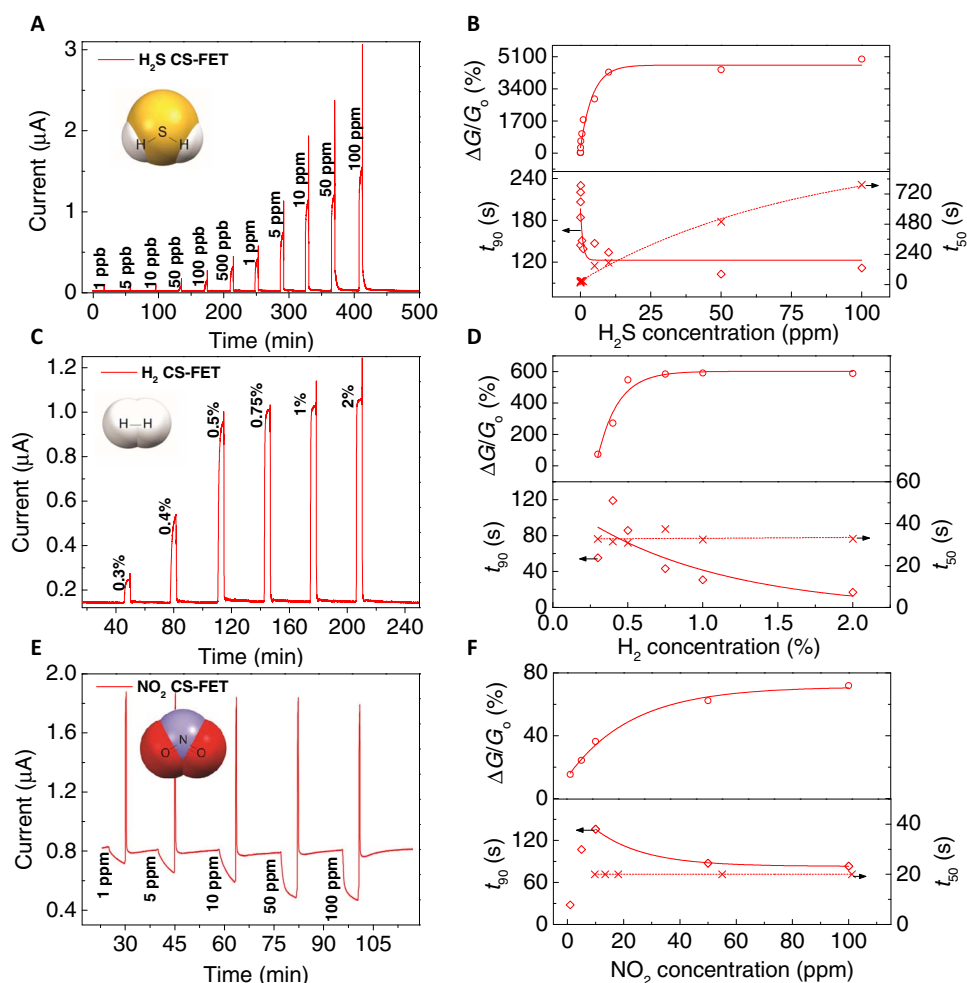


**Fig. 3. Experimental characterization of individual CS-FETs.** (A and B) Sensor response characteristics of a H<sub>2</sub>S-sensitive Pd-Au CS-FET ( $V_{DS} = 100$  mV;  $V_{BG} = 0$  V; relative humidity, ~30 to 40%;  $T \approx 25^\circ\text{C}$ ). (C and D) Sensor response characteristics of a H<sub>2</sub>-sensitive Ni-Pd CS-FET ( $V_{DS} = 2.5$  mV;  $V_{BG} = 0$  V; relative humidity, ~30 to 40%; and  $T \approx 25^\circ\text{C}$ ). (E and F) Sensor response characteristics of a NO<sub>2</sub>-sensitive Ni CS-FET ( $V_{DS} = 2.5$  mV;  $V_{BG} = 0$  V; relative humidity, ~45 to 50%;  $T \approx 25^\circ\text{C}$ ).

original baseline value after removal of gas) of H<sub>2</sub>S sensors increases with concentration, with ~20 s for 1 ppb of H<sub>2</sub>S and ~800 s for 100 ppm of H<sub>2</sub>S. A possible hypothesis for this is that H<sub>2</sub>S tends to strongly bond with the Pd-Au sensing layer, making it harder to desorb excess H<sub>2</sub>S molecules at larger concentrations (see fig. S4).

Similar to the H<sub>2</sub>S CS-FET sensor, the Ni-Pd-based H<sub>2</sub> sensor also exhibits linear and saturation characteristics in its time-dependent response curve (Fig. 3C). A supply voltage of 2.5 mV was used to drive the sensor at a baseline current of ~135 nA, consuming just ~0.34 nW of power. The lowest limit of detection is approximately 0.3% H<sub>2</sub> (~3000 ppm), with a saturation occurring above 0.5% H<sub>2</sub> (~5000 ppm) and a maximum sensitivity of 0.24%/ppm observed within this linear region. The interaction mechanism between H<sub>2</sub> and Ni-Pd is based on the dissociation and diffusion of the atomic hydrogen in palladium (27). Ni content in the sensing layer blocks H<sub>2</sub>S interaction with palladium (28), as will be demonstrated later. Compared to the H<sub>2</sub>S sensor, response times are much shorter with a minimum  $t_{90}$  of ~17 s for 2% H<sub>2</sub> (Fig. 3D). Microheater-assisted recovery time is also much shorter and is quite similar throughout the entire H<sub>2</sub> sensing range with a  $t_{50}$  of ~30 s.

In the case of the Ni sensing layer-based NO<sub>2</sub> sensor (Fig. 3E), baseline power consumption is ~2 nW based on a sensor current of

~820 nA at a supply voltage of 2.5 mV. Here, the CS-FET output current swings in the opposite direction compared to the H<sub>2</sub> and H<sub>2</sub>S sensor. As described previously, this indicates that the transistor  $V_t$  has increased (becomes more positive). The understanding here is that electron donation from NO<sub>2</sub> to the Ni sensing layer occurs because of its oxidizing nature. This makes the Ni sensing layer electronegative, leading to a decrease in its effective work function ( $-\Delta\phi$ ) and hence decreasing the potential of the capacitively coupled channel. Consequently, the transistor  $V_t$  becomes more positive and leads to a decrease in the CS-FET current ( $I_D$ ). As can be observed, the NO<sub>2</sub> CS-FET has a detection limit of 1 ppm and a saturation concentration of 50 ppm. The sensitivity of NO<sub>2</sub> is approximately 1%/ppm (Fig. 3F), and the minimum  $t_{90}$  is ~83 s for 100 ppm of NO<sub>2</sub>. Sensor recovery is near instantaneous with  $t_{50}$  dominated by the microheater on time (20 s).

As was previously discussed, the CS-FETs are fabricated using a top-down CMOS-compatible fabrication process that can facilitate the integration of large arrays of 3.5-nm-thin silicon channel transistors. Through multiple processing steps, different types of chemical-sensitive layers can be deposited on each transistor in an array, enabling a powerful multiplexed gas sensing platform. We demonstrate this using multiplexed H<sub>2</sub>S (Pd<sub>0.3nm</sub>Au<sub>1nm</sub>), H<sub>2</sub> (Ni<sub>0.3nm</sub>Pd<sub>1nm</sub>), and NO<sub>2</sub>

(Ni<sub>1mm</sub>) CS-FETs in Fig. 4, which is used to detect a sequence of eight gas pulses. Note that heat from the local microheaters manifests as current spikes in the CS-FET in response to temperature change during the recovery process, which is similar to that in Fig. 3. In this experiment, three successive 10-ppm H<sub>2</sub>S pulses were injected for 5 min, which were sensitively detected by the Pd-Au-based H<sub>2</sub>S CS-FET. The H<sub>2</sub> and NO<sub>2</sub> sensors had minimal effects due to the Ni content in sensing layers, which blocks any H<sub>2</sub>S interaction. Next, three consecutive injections of 0.5% H<sub>2</sub> pulses caused the Ni-Pd-based CS-FET to respond markedly. The NO<sub>2</sub> and H<sub>2</sub>S sensors showed only slight response to the 0.5% H<sub>2</sub> pulses, confirming their sensing layers as being relatively selective over hydrogen as well. Although the Pd-Au alloy-based sensing layer for the H<sub>2</sub>S CS-FET may respond to much larger concentrations of H<sub>2</sub>, theoretical and experimental works have hypothesized that Pd-Au clusters tend to interact weakly with H<sub>2</sub> compared to pure Pd (29, 30). To further check the selectivity between the three CS-FETs, we sequentially carried out 10-min mixed-gas test of H<sub>2</sub>S and H<sub>2</sub>. For the first 5 min, we injected 10 ppm of H<sub>2</sub>S from the H<sub>2</sub>S delivery line, and only dry air from the hydrogen delivery line was flowing. A 0.5% H<sub>2</sub> pulse was then injected for the next 5 min in the H<sub>2</sub>S ambient. As observed, the H<sub>2</sub>S and H<sub>2</sub> CS-FET sensors were able to respond to their respective target gases. During this mixed-gas test, the NO<sub>2</sub> CS-FET sensor responded minimally. Toward the end of the multiplexed measurements, a 100-ppm NO<sub>2</sub> pulse was injected for 5 min, which was quickly picked up by the Ni-based NO<sub>2</sub> CS-FET. The H<sub>2</sub> and H<sub>2</sub>S sensors responded minimally to NO<sub>2</sub>, with a decrease in

sensor currents. After each detection event, the local microheaters of all three CS-FETs were turned on simultaneously to recover and reset to sensor baseline.

On the basis of the results in Figs. 3 and 4, the silicon CS-FET framework provides a unique platform that can be used to integrate multiple gas sensors onto a single chip, beyond the three gases of interest in this work. Furthermore, the low power consumption of the underlying 3.5-nm-thin silicon transistor makes it possible for integration with mobile wireless electronics. To demonstrate this, we present a proof-of-concept application of our CS-FET gas sensor technology by integrating a H<sub>2</sub>-sensitive CS-FET sensor onto a wireless drone (Fig. 5). There is significant interest in unmanned aerial vehicle-based aerial mapping of harmful chemicals in the environment for threat detection/neutralization and ozone mapping, with a few early attempts using metal-oxide semiconductor gas sensors (31). Here, we used an off-the-shelf microdrone equipped with an ARM Cortex microprocessor, an inertial measurement unit, a barometric pressure sensor, and a radio frequency (RF) communication link (Crazyflie 2.0) (Fig. 5A). The Ni-Pd H<sub>2</sub>-sensitive CS-FET was integrated onto this drone using a simple voltage divider circuit. In a contained environment, a controlled leak of pure H<sub>2</sub> was carried out (estimated resulting concentration in air, ~1%). The test environment is shown in Fig. 5B, where the drone was tethered to high tension strings on either of its sides, such that its flight path was restricted in the vertical direction (*z* axis) only. A pre-programmed flight path was defined from a laptop that is enabled with an RF transceiver, where the drone would take off and climb at a steady

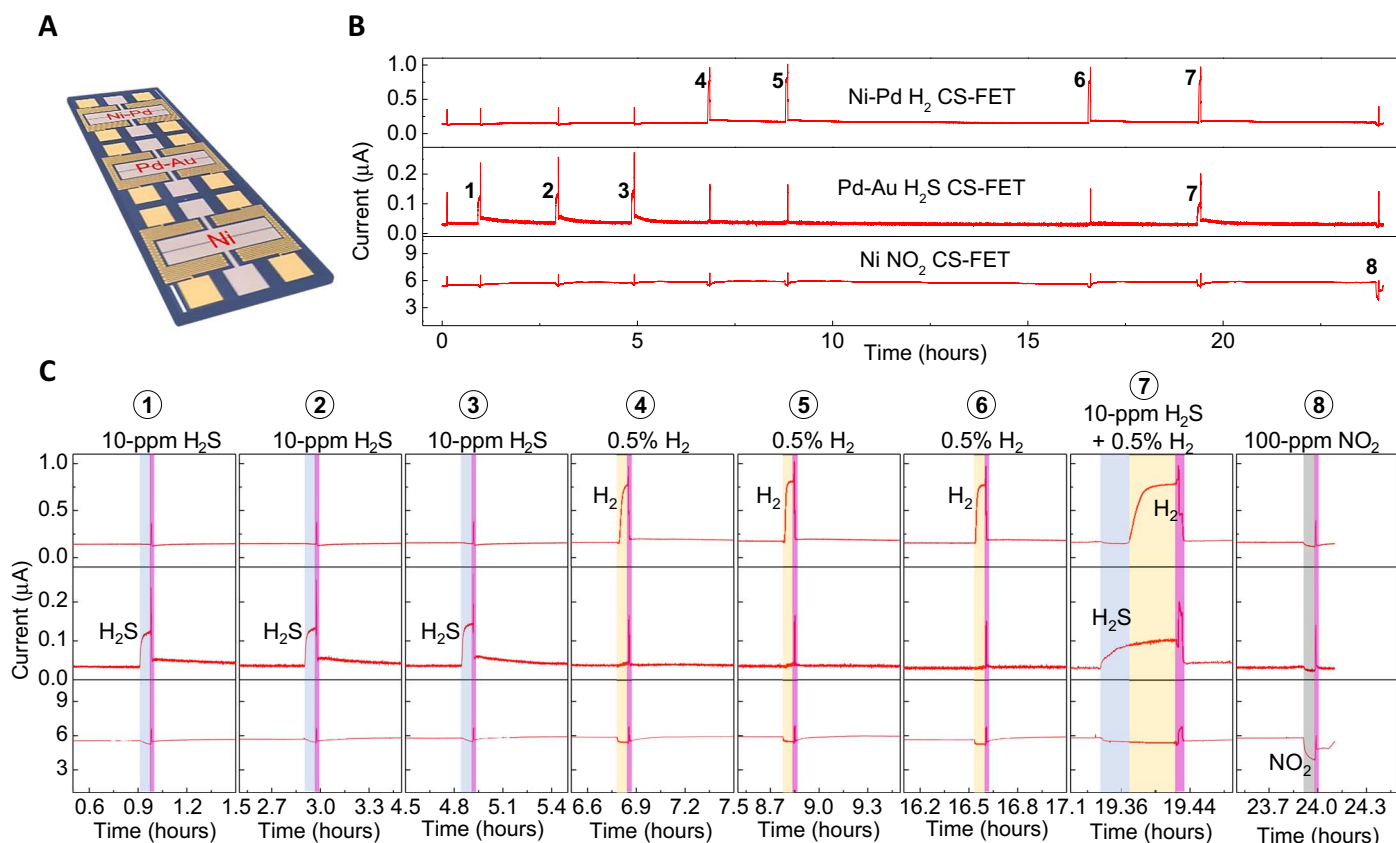


**Fig. 4. Multigas sensing using multiplexed CS-FETs.** (A) Optical microscopy image of a single CS-FET array chip. Scale bar, 200  $\mu\text{m}$ . (B) Real-time multiplexed sensing data to different gases ( $V_{\text{DS}} = 25$  mV;  $V_{\text{BG}} = 0$  V; relative humidity,  $\sim 40\%$ ;  $T \approx 25^\circ\text{C}$ ). (C) Close-up snippets of individual detection events in (B).

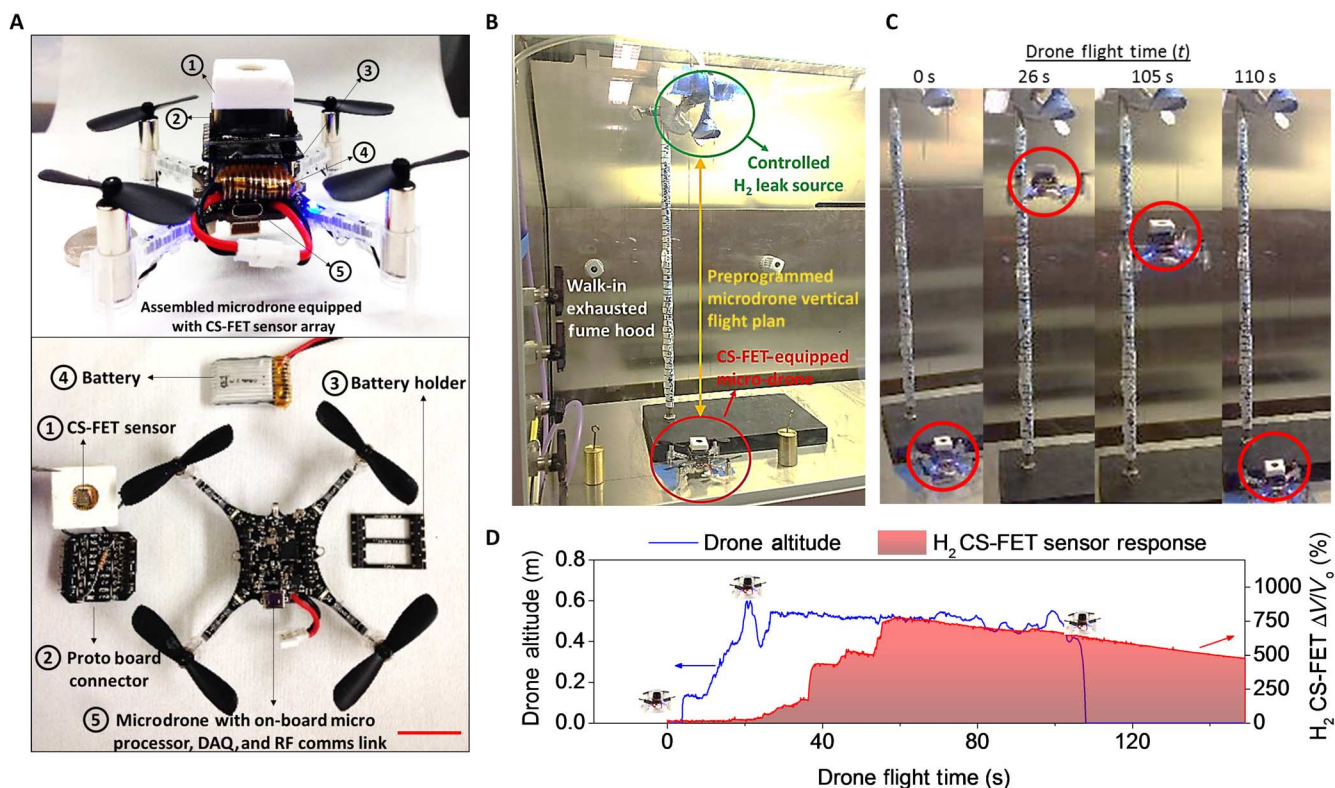


**Fig. 5. Aerial chemical sensing probes.** (A) Image showing a microdrone equipped with a Ni-Pd-based H<sub>2</sub>-sensitive CS-FET (top) and an unassembled drone showing the individual components (bottom). DAQ, data acquisition. (B) Image depicting the experimental setup used for the aerial hydrogen sensing experiment. (C and D) Image capture of the CS-FET-equipped microdrone in motion at different times with corresponding altimetry and generated H<sub>2</sub> sensor response, respectively.

rate to the source of the hydrogen leak, hover for a set period, and then descend, all while transmitting back the raw sensor data, as indicated in Fig. 5C. Figure 5D shows the real-time H<sub>2</sub> sensor measurement result and altimetry data corresponding to the experiment in Fig. 5C. Note that, because this was a proof-of-concept demonstration, no attempt was made to calibrate the raw sensor data. Furthermore, microheaters were not used for sensor recovery, indicating the slow H<sub>2</sub> sensor recovery to baseline at the end of the experiment.

## DISCUSSION

We have shown the CS-FET technology as a sensitive, selective, and low-power gas sensing platform based on ultrathin silicon channel transistors using conventional CMOS processing. Because of its relatively inert nature, pristine silicon can be engineered to be selective to a wide variety of gases. Using this, we have shown the possibility of contextual selectivity and multiplexed gas sensing by using CS-FETs functionalized with sub-5-nm metallic sensing layers, Pd-Au, Ni-Pd, and Ni, that are selective to three target gases, H<sub>2</sub>S, H<sub>2</sub>, and NO<sub>2</sub>, respectively, over each other. Finally, as a proof of concept for integration with mobile electronics, we demonstrated a H<sub>2</sub>-sensitive CS-FET integrated with a wireless microdrone for aerial detection of hydrogen.

From a practical large-scale fabrication standpoint, thickness uniformity control of the SOI wafers is an important challenge to the ultrathin silicon CS-FET technology presented here. However, the silicon integrated circuit (IC) industry is already addressing this, where these ultrathin and fully depleted SOI wafers are being explored to develop next-generation low-power digital electronics. From an economic

perspective, the cost of these devices will be minimal compared to the silicon IC industry because advanced nanofabrication processing techniques are not required for the CS-FET gas sensor technology. The final cost will be determined by chip size, number of chips per wafer, and packaging. In summary, our silicon CS-FET gas sensor platform can provide a robust platform for the research and development of new sensing layers for a wide variety of target chemicals, which will enable multigas detection on a single chip and at low power, paving way to applications in environmental pollution mapping and personal air-quality monitors.

## MATERIALS AND METHODS

### Sensor fabrication process flow

The starting substrates, <100> SOI wafers 200 mm in diameter, were used for CS-FET fabrication, which were procured from Soitec, with 70-nm-thick top silicon, 145-nm-thick buried oxide, and 725- $\mu$ m-thick silicon handle wafer. The active top silicon layer has a thickness variation of  $\pm 7.5$  nm. Both the top silicon and handle wafer silicon were lightly boron (p<sup>-</sup>)-doped, with a starting resistivity range of 8.5 to 11.5 ohm-cm. All experiments, except fig. S5, were carried out with devices made from these Soitec wafers. New and different devices were used each time for all experiments. All fabrication steps of the CS-FET sensor devices were carried out in an academic laboratory, because of which there are variations in channel thickness and doping concentration, resulting in sensor response and sensitivity variation. The CS-FET sensors for the experiment in fig. S5 were made using 300-mm <100> SOI wafers procured from Shin-Etsu with a 12-nm-thick top silicon layer (resistivity,

9 to 18 ohm-cm; boron), a 145-nm-thick buried oxide, and a 775-nm-thick silicon handle wafer (resistivity, 9 to 18 ohm-cm; boron).

The fabrication process is depicted in fig. S6. To achieve ultrathin silicon on insulator transistors, the initial 70-nm top silicon of the SOI wafer was trimmed by oxidation (Tystar furnaces) at 1000°C in atmosphere using a three-step dry (5 min)–wet (13:45 min)–dry (5 min) process. This ensured rapid oxidation with a resultant low-stress SiO<sub>2</sub> and a clean SiO<sub>2</sub>/Si interface. After this, a dilute (1:10) hydrofluoric acid (HF) solution was used to strip the grown oxide, leaving a thin top silicon layer. Six-point, fixed-angle (70°) ellipsometry indicated that the top silicon average thickness was approximately 5 to 6 nm, which was later confirmed to be approximately 3.5 nm under TEM. After this, 250-μm-long and 5-μm-wide mesas were patterned using i-line photolithography with a clear field quartz mask and image reversal photoresist (MicroChemicals GmbH AZ nLOF 2020). Next, using a TCP Poly-Si etcher (Lam Research Corp.), silicon etching in Cl<sub>2</sub> and HBr completed thin-body silicon mesa etching. The etching process resulted in a slight over-etch in the buried oxide (<10 nm). Postetching, the photoresist atop the silicon mesa patterns, was removed in acetone. An ensuing wet cleanse was performed in a standard peroxide (Piranha) mixture at 120°C followed by a 10-s dilute HF (1:10) dip. Source/drain (S/D) contacts were then defined with physical gate lengths (S/D separation) of 2 and 5 μm. Ni (50 nm) was deposited using thermal evaporation, before which the wafers were stripped of native SiO<sub>2</sub> in a 1:50 dilute HF solution for 20 s. Ni lift-off was carried out in acetone after which the wafers were annealed in forming gas at 350°C for 1 min to form a nickel silicide (NiSi). After this, microheater patterns were defined adjacent to the CS-FETs, after which Au (400 nm)/Cr (20 nm) was deposited by electron beam evaporation followed up lift-off in acetone. Functionalization of individual CS-FETs was carried out by a sequential blanket evaporation of different materials using a combination of thermal and electron beam, at a very slow rate (~0.1 to 0.2 Å/s) at room temperature. No annealing or chemical treatment was carried out on the sensing layers and was used as deposited.

### Sensor measurement apparatus and setup

To ensure health and safety, all gas sensing measurements were carried out in a walk-in fume hood. The CS-FET chip was wire-bonded to a 64-pin chip carrier. Different power supply sources were used for the CS-FET sensor devices and the individual microheaters, with all CS-FETs tied to a common ground and the individual microheaters tied to a different common ground. The chip carrier containing the CS-FET sample was housed in a three-dimensional printed minichamber (47 mm × 47 mm × 23 mm) made of chemically resistant polylactic acid, with just enough room to house the CS-FET chip carrier. Synthetic air-diluted H<sub>2</sub>S and NO<sub>2</sub> gas cylinders were purchased from MESA International Technologies Inc. at a calibrated concentration. For H<sub>2</sub> sensing experiments, ultrahigh purity hydrogen (Praxair Technology Inc.) was used and diluted with house-compressed dry air. Typical gas flow rates were from 1 to 100 sccm, and diluent (air) flow rate was approximately 1000 sccm. Humidity and temperature in the ambient were monitored by a commercial sensor purchased from Sensirion AG (Model SHT2x). Gas delivery was controlled by mass flow controllers (Alicat Scientific Inc.) and manual flow meters (Dwyer Instruments Inc., Matheson Tri-Gas). A current preamplifier (Keithley 428) was used to set the bias power of the CS-FETs, and the sensor signal was collected via a computer-controlled data acquisition board (National Instruments, NI USB-6259). Multiplexed sensing experiments were achieved through relays with a sample rate of 1 Hz. A separate power

source (Agilent E3631A) was used to drive the microheaters. This setup was used to obtain the time-dependent sensor measurements of each of the CS-FETs shown in Fig. 3 that were then used to determine their individual performance metrics pertaining to sensor response ( $\Delta G/G_0$ ), response time ( $t_{90}$ ; time taken for the sensor to reach 90% of its peak value from baseline), and recovery time ( $t_{50}$ ; time taken for the sensor to recover within 50% of its initial baseline). After each gas exposure, the gas line was physically disconnected from the minichamber and microheater recovery carried out in the fume hood ambient. In the multiplexed gas sensing experiment (Fig. 4), the integrated microheaters of all CS-FETs were turned on simultaneously after each gas exposure for a 20-s period with a draw current of 100 mA from each individual heater.

### SUPPLEMENTARY MATERIALS

Supplementary material for this article is available at <http://advances.sciencemag.org/cgi/content/full/3/3/e1602557/DC1>

- S1. Sensor characteristics of an unfunctionalized CS-FET sensor
- S2. Nanoparticle sensing layer sparsity analysis
- S3. Effect of silicon channel thickness on CS-FET sensitivity
- S4. CS-FET sensor response to temperature, relative humidity, and room temperature recovery characteristics
- S5. Individual sensor cycling from low and high gas concentrations
- S6. Fabrication process of chemical-sensitive 3.5-nm-thin silicon transistors
- S7. Microheater characterization
- S8. Transfer characteristics of H<sub>2</sub>S, H<sub>2</sub>, and NO<sub>2</sub> CS-FETs
- fig. S1. Properties of a control CS-FET without any sensing film.
- fig. S2. Top-down TEM image of an ultrathin Pd<sub>0.3nm</sub>Au<sub>1nm</sub> on Si<sub>3</sub>N<sub>4</sub> grids.
- fig. S3. CS-FET sensor response dependence on silicon channel thickness.
- fig. S4. Influence of ambient temperature and humidity on CS-FET sensor response.
- fig. S5. High-low-high gas concentration cycling of CS-FET sensors.
- fig. S6. CMOS-compatible fabrication process of CS-FETs.
- fig. S7. Integrated microheater material selection and characterization.
- fig. S8. Typical electrical transfer characteristics ( $I_D$ - $V_{BG}$ ) of functionalized CS-FETs.

### REFERENCES AND NOTES

1. A. Ponzoni, E. Comini, G. Sberveglieri, J. Zhou, S. Z. Deng, N. S. Xu, Y. Ding, Z. L. Wang, Ultrasensitive and highly selective gas sensors using three-dimensional tungsten oxide nanowire networks. *Appl. Phys. Lett.* **88**, 203101 (2006).
2. X. Li, Y. Lu, J. C. Hemminger, R. M. Penner, Catalytically activated palladium@platinum nanowires for accelerated hydrogen gas detection. *ACS Nano* **9**, 3215–3225 (2015).
3. M. Li, H. X. Tang, M. L. Roukes, Ultra-sensitive NEMS-based cantilevers for sensing, scanned probe and very high-frequency applications. *Nat. Nanotechnol.* **2**, 114–120 (2007).
4. M. C. McAlpine, H. Ahmad, D. Wang, J. R. Heath, Highly ordered nanowire arrays on plastic substrates for ultrasensitive flexible chemical sensors. *Nat. Mater.* **6**, 379–384 (2007).
5. J. Kong, N. R. Franklin, C. Zhou, M. G. Chapline, S. Peng, K. Cho, H. Dai, Nanotube molecular wires as chemical sensors. *Science* **287**, 622–625 (2000).
6. P. Qi, O. Vermesh, M. Greco, A. Javey, Q. Wang, H. Dai, Towards large arrays of multiplex functionalized carbon nanotube sensors for highly sensitive and selective molecular detection. *Nano Lett.* **3**, 347–351 (2003).
7. K. A. Mirica, J. M. Azzarelli, J. G. Weiss, J. M. Schnorr, T. M. Swager, Rapid prototyping of carbon-based chemiresistive gas sensors on paper. *Proc. Natl. Acad. Sci. U.S.A.* **110**, E3265–E3270 (2013).
8. S. F. Liu, S. Lin, T. M. Swager, An organocobalt–carbon nanotube chemiresistive carbon monoxide detector. *ACS Sens.* **1**, 354–357 (2016).
9. J. Li, Y. Lu, Q. Ye, L. Delzeit, M. Meyyappan, A gas sensor array using carbon nanotubes and microfabrication technology. *Electrochem. Solid-State Lett.* **8**, H100–H102 (2005).
10. Y. Cui, Q. Wei, H. Park, C. M. Lieber, Nanowire nanosensors for highly sensitive and selective detection of biological and chemical species. *Science* **293**, 1289–1292 (2001).
11. E. Stern, J. F. Klemic, D. A. Routenberg, P. N. Wyrembak, D. B. Turner-Evans, A. D. Hamilton, D. A. LaVan, T. M. Fahmy, M. A. Reed, Label-free immunodetection with CMOS-compatible semiconducting nanowires. *Nat. Mater.* **445**, 519–522 (2007).
12. J.-W. Han, T. Rim, C.-K. Baek, M. Meyyappan, Chemical gated field effect transistor by hybrid integration of one-dimensional silicon nanowire and two-dimensional tin oxide thin film for low power gas sensor. *ACS Appl. Mater. Interfaces* **7**, 21263–21269 (2015).

13. J.-H. Ahn, J. Yun, Y.-K. Choi, I. Park, Palladium nanoparticle decorated silicon nanowire field-effect transistor with side-gates for hydrogen gas detection. *Appl. Phys. Lett.* **104**, 013508 (2014).
14. N. Shehada, G. Brönstrup, K. Funka, S. Christiansen, M. Leja, H. Haick, Ultrasensitive silicon nanowire for real-world gas sensing: Noninvasive diagnosis of cancer from breath volatolome. *Nano Lett.* **15**, 1288–1295 (2015).
15. J. Nah, S. B. Kumar, H. Fang, Y.-Z. Chen, E. Plis, Y.-L. Chueh, S. Krishna, J. Guo, A. Javey, Quantum size effects on the chemical sensing performance of two-dimensional semiconductors. *J. Phys. Chem. C* **116**, 9750–9754 (2012).
16. O. Knopfmacher, M. L. Hammock, A. L. Appleton, G. Schwartz, J. Mei, T. Lei, J. Pei, Z. Bao, Highly stable organic polymer field-effect transistor sensor for selective detection in the marine environment. *Nat. Commun.* **5**, 2954 (2014).
17. T. Gao, M. D. Woodka, B. S. Brunschwig, N. S. Lewis, Chemiresistors for array-based vapor sensing using composites of carbon black with low volatility organic molecules. *Chem. Mater.* **18**, 5193–5202 (2006).
18. J. Janata, M. Josowicz, Organic semiconductors in potentiometric gas sensors. *J. Solid State Electrochem.* **13**, 41–49 (2009).
19. F. Schedin, A. K. Geim, S. V. Morozov, E. W. Hill, P. Blake, M. I. Katsnelson, K. S. Novoselov, Detection of individual gas molecules adsorbed on graphene. *Nat. Mater.* **6**, 652–655 (2007).
20. S. Cui, H. Pu, S. A. Wells, Z. Wen, S. Mao, J. Chang, M. C. Hersam, J. Chen, Ultrahigh sensitivity and layer-dependent sensing performance of phosphorene-based gas sensors. *Nat. Commun.* **6**, 8632 (2015).
21. A. N. Abbas, B. Liu, L. Chen, Y. Ma, S. Cong, N. Aroonyadet, M. Köpf, T. Nilges, C. Zhou, Black phosphorus gas sensors. *ACS Nano* **9**, 5618–5624 (2015).
22. H. Jang, W. Lee, S. M. Won, S. Y. Ryu, D. Lee, J. B. Koo, S.-D. Ahn, C.-W. Yang, M.-H. Jo, J. H. Cho, J. A. Rogers, J.-H. Ahn, Quantum confinement effects in transferrable silicon nanomembranes and their applications on unusual substrates. *Nano Lett.* **13**, 5600–5607 (2013).
23. Y.-K. Choi, D. Ha, T.-J. King, C. Hu, Nanoscale ultrathin body pMOSFETs with raised selective germanium source/drain. *IEEE Electron Device Lett.* **22**, 447–448 (2001).
24. Centers for Diseases Control and Prevention, [www.cdc.gov/niosh](http://www.cdc.gov/niosh) [accessed 24 December 2016].
25. J. F. Fennell Jr., S. F. Liu, J. M. Azzarelli, J. G. Weis, S. Rochat, K. A. Mirica, J. B. Ravnshæk, T. M. Swager, Nanowire chemical/biological sensors: Status and a roadmap for the future. *Angew. Chem. Int. Ed.* **55**, 1266–1281 (2016).
26. J.-P. Colinge, C.-W. Lee, A. Afzalian, N. D. Akhavan, R. Yan, I. Ferain, P. Razavi, B. O'Neill, A. Blake, M. White, A.-M. Kelleher, B. McCarthy, R. Murphy, Nanowire transistors without junctions. *Nat. Nanotechnol.* **5**, 225–229 (2010).
27. H. Conrad, G. Ertl, E. E. Latta, Adsorption of hydrogen on palladium single crystal surfaces. *Surf. Sci.* **41**, 435–446 (1974).
28. R. C. Hughes, W. K. Schubert, R. J. Buss, Solid-state hydrogen sensors using palladium-nickel alloys: Effect of alloy composition on sensor response. *J. Electrochem. Soc.* **142**, 249–254 (1995).
29. M. E. Björketun, G. S. Karlberg, J. Rossmels, I. Chorkendorff, H. Wolfschmidt, U. Stimming, J. K. Nørskov, Hydrogen evolution on Au(111) covered with submonolayers of Pd. *Phys. Rev. B* **84**, 045407 (2011).
30. A. Roudgar, A. Groß, Local reactivity of supported metal clusters: Pd<sub>n</sub> on Au(111). *Surf. Sci.* **559**, L180–L186 (2004).
31. A. Khan, D. Schaefer, L. Tao, D. J. Miller, K. Sun, M. A. Zondlo, W. A. Harrison, B. Roscoe, D. J. Lary, Low power greenhouse gas sensors for unmanned aerial vehicles. *Remote Sens.* **4**, 1355–1368 (2012).

**Acknowledgments:** We are grateful to K. Chen, S. B. Desai, A. B. Sachid, S.-Y. Cho, T. Rembert, H. Y. Y. Nyein, and J. Bullock for their help and useful comments. We are grateful to C. C. Hu for the insightful discussions in developing the underlying silicon transistor. We thank Emerson/Rosemount for valuable feedback on CS-FET sensor characterization. We also thank the Marvell Nanofabrication Laboratory staff for their help and suggestions. **Funding:** This work was jointly funded by the U.S. NSF (PFI:AIR-TT program), Chevron Corporation, and Murata Manufacturing Company Limited. Y.-L.C. was funded by the Ministry of Science and Technology (grants 105-3113-E-007-003-CC2, 104-2628-M-007-004-MY3, 104-2221-E-007-048-MY3, 105-2633-M-007-003, and 104-2622-M-007-002-CC2) and the National Tsing Hua University (grant 105A0088J4). **Author contributions:** A.J. conceived and supervised the project. H.M.F. led the project. H.M.F. and H.S. equally carried out all fabrication and characterization of CS-FET sensors. M.A. helped with the data acquisition setup. H.M.F. and H.S. designed the gas sensor characterization setup with help from M.H. and H.O. C.Z. and V.S.H. carried out the microdrone experiment. W.G. and D.K. helped with the sensing layer development. Y.-Z.C. and Y.-L.C. helped with top-down TEM characterization of the Pd-Au sensing layer. All the authors discussed the results and wrote the paper. **Competing interests:** The authors declare that they have no competing interests. **Data and materials availability:** H.F., H.S., and A.J. filed a patent related to this work with the University of California, Berkeley, through the U.S. Patents Office application PCT/US2015/034068 (filing date, 03 June 2015). All data needed to evaluate the conclusions in the paper are present in the paper and/or the Supplementary Materials. Additional data related to this paper may be requested from the authors.

Submitted 18 October 2016

Accepted 9 February 2017

Published 24 March 2017

10.1126/sciadv.1602557

**Citation:** H. M. Fahad, H. Shiraki, M. Amani, C. Zhang, V. S. Hebbar, W. Gao, H. Ota, M. Hettick, D. Kiriya, Y.-Z. Chen, Y.-L. Chueh, A. Javey, Room temperature multiplexed gas sensing using chemical-sensitive 3.5-nm-thin silicon transistors. *Sci. Adv.* **3**, e1602557 (2017).

This article is published under a Creative Commons license. The specific license under which this article is published is noted on the first page.

For articles published under [CC BY](#) licenses, you may freely distribute, adapt, or reuse the article, including for commercial purposes, provided you give proper attribution.

For articles published under [CC BY-NC](#) licenses, you may distribute, adapt, or reuse the article for non-commercial purposes. Commercial use requires prior permission from the American Association for the Advancement of Science (AAAS). You may request permission by clicking [here](#).

**The following resources related to this article are available online at <http://advances.sciencemag.org>. (This information is current as of March 27, 2017):**

**Updated information and services**, including high-resolution figures, can be found in the online version of this article at:

<http://advances.sciencemag.org/content/3/3/e1602557.full>

**Supporting Online Material** can be found at:

<http://advances.sciencemag.org/content/suppl/2017/03/20/3.3.e1602557.DC1>

This article **cites 29 articles**, 5 of which you can access for free at:

<http://advances.sciencemag.org/content/3/3/e1602557#BIBL>

*Science Advances* (ISSN 2375-2548) publishes new articles weekly. The journal is published by the American Association for the Advancement of Science (AAAS), 1200 New York Avenue NW, Washington, DC 20005. Copyright is held by the Authors unless stated otherwise. AAAS is the exclusive licensee. The title *Science Advances* is a registered trademark of AAAS